A computational method for determining combined ductility demands on steel structures subject to multi-hazards

Song, Jing; Skalomenos, Konstantinos; Martinez-Vazquez, Pedro; Kastiza, Pelagia

ICONHIC2022
3rd International Conference on Natural Hazards & Infrastructure
5-7 July 2022, Athens, Greece

A computational method for determining combined ductility demands on steel structures subject to multi-hazards

Jing Song, Konstantinos Skalomenos, Pedro Martinez-Vazquez, Pelagia Kastiza
Department of Civil Engineering, Edgbaston, Birmingham, B15 2TT, University of Birmingham

ABSTRACT

This paper presents a computational method for investigating the ductility demands induced by thunderstorm downbursts to steel building structures that have been previously damaged during a strong hazard event of any nature (earthquakes, strong winds). The proposed computational method synchronizes the finite element (FE) analysis software ABAQUS and MATLAB reverse optimization subroutines. A nonlinear static pushover analysis is initially performed to induce the ductility demands of the first hazard event and identify the relationship between the base shear force and lateral roof drift up to a target plastic deformation. The method uses the pushover analysis in order to bring the structure at a pre-defined ductility level, including the descending branch of the load-deformation curve, thus allowing for a direct control of the initially imposed damage. The transient non-stationary wind loads are then subsequently applied as an externally applied dynamic loading and the revised displacement ductility demand is directly determined. The method is applied on a tall steel building subject to several initial damage stages and three subsequent thunderstorm downburst synthetic records. The results demonstrate the non-negligible effects of such wind events on the total ductility demands. The method can successfully quantify the increased ductility demands on structures subjected to multi-hazards.

Keywords: Thunderstorm downburst, Ductility demand, Sequential hazards, Non-linear analysis

1. INTRODUCTION

The devastating effects of severe thunderstorms observed over the last decades has motivated researchers to study this complex phenomenon (Brooks, 2013; Rädler et al., 2019). Factual evidence shows that building structures that have absorbed damage during previous hazard events (earthquake, strong wind) are prone to secondary effects induced by sequential hazards, such as thunderstorm downbursts (ABCNEWS, 2017; CNN, 2017). This may increase post-disaster damages and eventually cause the collapse of structures that remained exposed after the primary hazard.

A thunderstorm downburst distinguishes from synoptic winds as it produces small-scale flow divergence within radius of 4 km accompanied with intense microbursts. This configuration can cause damage equivalent to synoptic wind flow of 75 m/s, within a time interval ranging 5 - 20 min (Fujita, 1985; Lombardo et al., 2014). Due to the 'nose shape' profile with varying height above the ground, the wind speed peaks between 30 - 100 m height above the ground (Fujita, 1990). This phenomenon imposes risks associated to the collapse mechanism of tall structures (Loredo-Souza et al., 2019; Tilloy et al., 2019). The state of the art still identifies important knowledge gaps spanning from the design aspects to the development of contingency plans and strategies to increase resilience. The current guidance evidences such limitations as these disregards the joint occurrence of natural events such as earthquakes and wind (Aly and Abburu, 2015; Duthinh and Simiu, 2010; Thilakarathna et al., 2018). Recently, Kwag et al. (2021) proposed a design framework considering seismic load and strong synoptic wind. Further studies have focused on managing multi-hazards (Elias et al., 2019;

Taha, 2021), although to date no research has been done to determine the ductility demands on damaged structures under additional effects of thunderstorm downbursts.

This paper investigates the effects of the downburst outflow wind on the ductility demands of damaged buildings. The proposed methodology combines the principles of the nonlinear adaptive static (pushover) analysis (Chopra and Goel, 2002) which aims to reproduce the damage induced by the primary hazard event, with the sequential dynamic analysis (Isobe and Tanaka, 2021; Li and Ellingwood, 2007; Martinez-Vazquez et al., 2019; Park et al., 2012) which aims to estimate the damage induced by the secondary sequential thunderstorm event. Based on the initial study of Skalomenos and Papazafeiropoulos (2019), the proposed algorithm offers a robust implementation of pushover analysis and superior numerical results can be obtained, especially the descending branch of the pushover curve and collapse mechanism. The computational procedure proposed in this paper combines the step-by-step nonlinear adaptive pushover analysis with the dynamic time history analysis within a restart analysis framework to obtain the base shear - roof displacement relationship for different damage levels. Accordingly, the global plastic deformation mechanism that leads to collapse can be identified. The new computational algorithm is applied on a tall steel building structure subject in its damaged stage to three downburst synthetic records. The results demonstrate the non-negligible effects of such wind events on the ductility demands of damaged structures.

2. METHODOLOGY

The following algorithm builds ABAQUS (2020) pushover capabilities in MATLAB (2021). Through a static analysis with mixed force/displacement control, the method can trace the descending branch of the structural response without using Riks analysis (Skalomenos and Papazafeiropoulos, 2019). Static analysis with arc-length control (Riks) can trace only a single loading path during the analysis and does not allow the user to control over the force distribution pattern during the pushover analysis.

During the initial loading process, each storey of the model building has assigned one control point connected to other points via shear springs that simulate diaphragmatic flexibility. The gravity loads are applied as point loads on nodal coordinates to reflect P-Δ effects. The first step is thus the axial load analysis, followed by the frequency analysis which provides lateral coordinate distribution of the first modal shape. A standard modal mass algorithm yields the adaptive force distribution (Chopra and Goel, 2002).

ABAQUS offers the capability of the restart analysis. This helps to develop a sequential-hazard analysis through restarting the pushover lateral displacement analysis to implement the force/displacement control. The target displacement assigned at the top of the structure guides the determination of the acting shear per storey through a reverse optimization procedure based on the force pattern associated with the fundamental mode of vibration. This method could be extended to add contributions to all meaningful modes of vibration. The load-displacement optimization process is explained below (Skalomenos and Papazafeiropoulos, 2019).

Each increment (i) of the optimization procedure maps the linear dependence between the real force distribution imposed at the building, $\{F_{r,i}\}$, and target force distribution created by its fundamental eigenmode, $\{F_{t,i}\}$, using a load proportionality factor, λ_i, implicit in Eq. (1).

$$F_{r,i}(n) = \lambda_i F_{t,i}(n), n = 1,2,\dots N \tag{1}$$

In this equation, N is the total number of storeys.

According to the controlled roof displacement and real force on the rest of the storey, the reaction force at the roof level can be obtained to minimize the variance of the ratio between the real force array and the target array (see Eq. (2)) within the loop until $d \cong 0$.

$$d = var(\{F_{r,i}\} / \{F_{t,i}\}) \tag{2}$$

The advantage of this procedure is that the subsequent analysis step can be implemented based on any previous steps even in the stage of plastic range. This helps to restart the subsequent analysis under the downburst outflow wind loads (secondary hazard event) after the building has reached a pre-defined ductility level (primarily hazard event). The restart wind analysis is a force control dynamic analysis using the implicit dynamic analysis algorithm available in ABAQUS. The dynamic analysis starts after the adaptive non-linear pushover analysis has stopped and the building returned to the zero-force equilibrium (permanent plastic deformations). The proposed multi-hazard analysis method can directly control the non-linear analysis steps and randomly combine different types of loads induced by multi-hazard events under variable load patterns. The computing displacement ductility demand is defined as the non-linear roof displacement divided by the yielding roof displacement of the overall structure.

3. INVESTIGATION ON HIGH-RISE BUILDING

3.1 Building information

A 20-storey high-rise building (see Figure 1 (a)) designed according to the Uniform Building Code (1994) is adopted here for investigation. The detailed design of this building is presented in Hall (2018). The height of the building is 74.11 m. The ground and first floor have 4.57 m height, while the rest floors have 3.66 m height. The plan view dimensions of the building are 36.6 m × 24.4 m with 6.1 m bay width in both directions. The terrain type for wind design is exposure B with a basic wind speed of 31 m/s and the soil type for the earthquake design is S2 within Zone 4. The seismic base shear coefficient is 0.03 while the drift limitation is 0.025. The gravity loads are 6.23 kPa for floors including cladding load and 3.59 kPa for the roof.

The lateral loads from pushover and wind load are applied in the short direction. Considering the symmetry of this building, this building consists of two parts, including one exterior moment resisting frame (MRF), and one interior equivalent gravity frame (GF) to represent half of the building and simulate the second order effects. These two frames are connected by Link types of multi-point constraints (MPC) which provide a pinned rigid link between the two frames at each storey level. The steel is modelled as a bilinear elastic isotropic material with modulus of elasticity E=210 GPa, density ρ=7850 kg/m^3 and Poisson ratio ν=0.3. The half weight of this building is 54.46 MN. The damping is omitted in the current stage. The yield strength of the steel is taken as 248 MPa and the ultimate strength is 400 MPa.

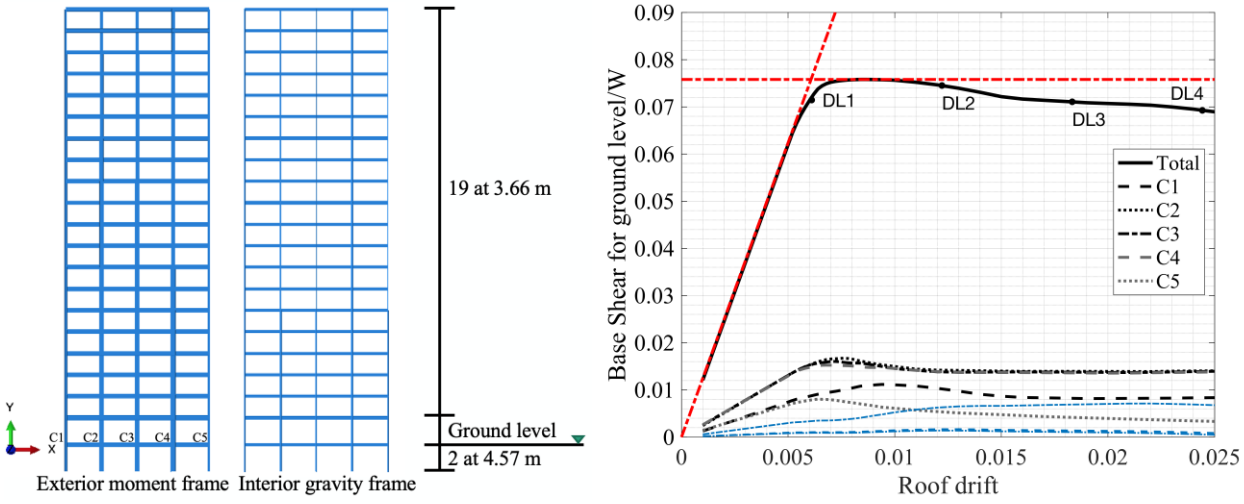

(a) (b)

Figure 1. *Basic information for building model, (a) Building dimensions; (b) Pushover curves.*

This building model has been built in ABAQUS with beam elements. All the columns in the interior gravity frame are defined by the generalized section properties. The sectional area and the moment of inertia in major and minor directions for the columns have been calculated as equivalent to half of the overall structure, i.e. 2.5

times of original values. The Link type of MPC has been chosen to connect the points on each storey to approximately represent diaphragm flexibility. All the points on each storey are controlled by the cross points in the first column of the building frame. The mass has been assigned on the top of the columns. The basement of this modelling frame has been fully constrained, and the ground floor has been constrained by the displacement in both directions. The beam connections in the exterior moment frame are fully fixed, and the beam connections in the interior gravity frame are fully pinned connections.

3.2 Model analysis

This procedure starts from the analysis of the axial loads and frequency analysis. The fundamental natural period of the building is 4.01 seconds which is higher than the value of 3.63 seconds from Hall (2018) since the beam connections of the gravity frame have been simulated as perfect pins.

According to the step-by-step restart static analysis of this building, the pushover curve can be obtained as shown in Figure 1 (b) which demonstrates the relationship between the roof drift and total column shear force at the ground level (base shear). The yielding point in the pushover curve can be defined by the intersection of the red lines, i.e. the total base shear to roof drift at the elastic range and the peak value of the total base shear at the maximum capacity of the structure. Then, the target ductility can be calculated for different ductility levels using Eq. (3),

$$DL = \frac{d_{target}}{d_{yielding}} \tag{3}$$

In this equation, d_{target} is the target roof drift (roof displacement divided by the total height of the building), and $d_{yielding}$ is the yielding drift. The d_{target} is 0.0061, 0.0122, 0.0182, 0.0244 for DL1, DL2, DL3 and DL4 damage state which corresponds to a roof displacement ductility of 1, 2, 3 and 4, respectively. The yielding drift $d_{yielding}$ is 0.0061. The base shear force - roof drift relationship of each column is shown in Figure 1 (b) where C1-C5 represents the column 1 to 5 from the left side of the moment frame.

3.3 Applied transient winds

In this paper, a hybrid theoretical procedure for developing an artificial downburst wind velocity field proposed by Chen and Letchford (2004) is adopted, which consists of three main steps: (1) generate random fluctuating velocity time series based on spectral representation (Priestley, 1965) using evolutionary power spectral density function and the detailed simulation process of the reduced turbulent fluctuation are presented by Deodatis (1996); (2) build the slowly varying mean velocity based on the vertical shape profile of horizontal wind proposed by Wood et al. (2001) and time function suggested by Holmes and Oliver (2000); (3) construct the total velocity time history of downburst outflow detailed at Chen and Letchford (2004), i.e. $U(z,t) = \overline{U}(z,t) + u'(z,t) = \overline{U}(z,t) + \sigma_u(z,t)\tilde{u}'(z,t) = \overline{U}(z,t) + I_u(z)\overline{U}(z,t)\tilde{u}'(z,t)$, where z is the height above the ground, t is the time, $\overline{U}$ is the slowly varying mean velocity, u' is the fluctuating wind velocity, σ_u is the slowly varying standard deviation, dealt with as a modulation function, $\tilde{u}'$ is the reduced turbulent fluctuation, dealt with as a rapid varying stationary Gaussian random field and I_u is the turbulence intensity. The power spectral density function proposed by Solari et al. (2015) is adopted in this study, as shown in Eq. 4.

$$\frac{nS_{\tilde{u}'}(z,n)}{{\sigma_u}^2(z)} = \frac{18\left(\frac{nz}{\overline{U}_{max(z)}}\right)}{\left[1+27\left(\frac{\omega z}{2\pi\overline{U}_{max(z)}}\right)\right]^{5/3}} \tag{4}$$

In Eq. (4), n is the frequency of gust wind, ω is the circular frequency and $\overline{U}_{max}$ is the maximum slowly varying mean velocity. Furthermore, due to the lack of data on effective vertical profiles of the turbulence intensity along with the height under thunderstorm downburst events, the profiles of turbulence intensity which is generally used for synoptic winds from the ASCE7 (2013) is used here. The cut-off circular frequency is assumed as 4 rad/s, and the number of circular frequency steps, N, is equal to 2048. It is reasonable to assume

a sampling frequency of the simulated fluctuation equal to 2.56 Hz. It should be noted that the reference velocity and reference height are taken from the peak value (36.5 m/s) of the slowly varying mean velocity at 13 m height with a 50-year return period (Solari et al., 2015; Solari et al., 2013). Accordingly, 20 velocity time histories are generated for each wind field, ranging from 4.75 m to 74.11 m with 3.66 m height increment (i.e. storey height) that correspond to each storey level of the building. The cross-spectral density of the turbulent fluctuating is considered in the simulation of the wind field; therefore, the wind effects on the enclosures of the building frame have been integrated to the concentrated load acting on the bearing elements of the structures.

The 3-second peak velocity time histories at the height of maximum velocity, i.e. $z_{U_{max}}$= 30 m, 50 m and 70 m above the ground, are demonstrated in Figure 2 (a). The maximum velocities, U_{max}, are 59 m/s, 63 m/s and 68 m/s for $z_{U_{max}}$=30 m, 50 m and 70 m, respectively. This defines three different velocity profiles along the building height, thus affecting the lateral input load distribution and energy absorption capacity of the building. The terrain category is exposure B. The transient wind loads are then calculated by $f = C_d \times 0.5\rho U(t)^2 A$ for each storey, imposed as concentrated load on each storey of the building frame. In this profile, C_d is assumed to equal to 1.2 (Melbourne, 1980), ρ is equal to 1.225 kg/m^3 and A is the storey area exposed to wind. The vertical velocity profiles of the horizontal wind are illustrated in Figure 2 (b) where the dash lines are the trendlines for each profile.

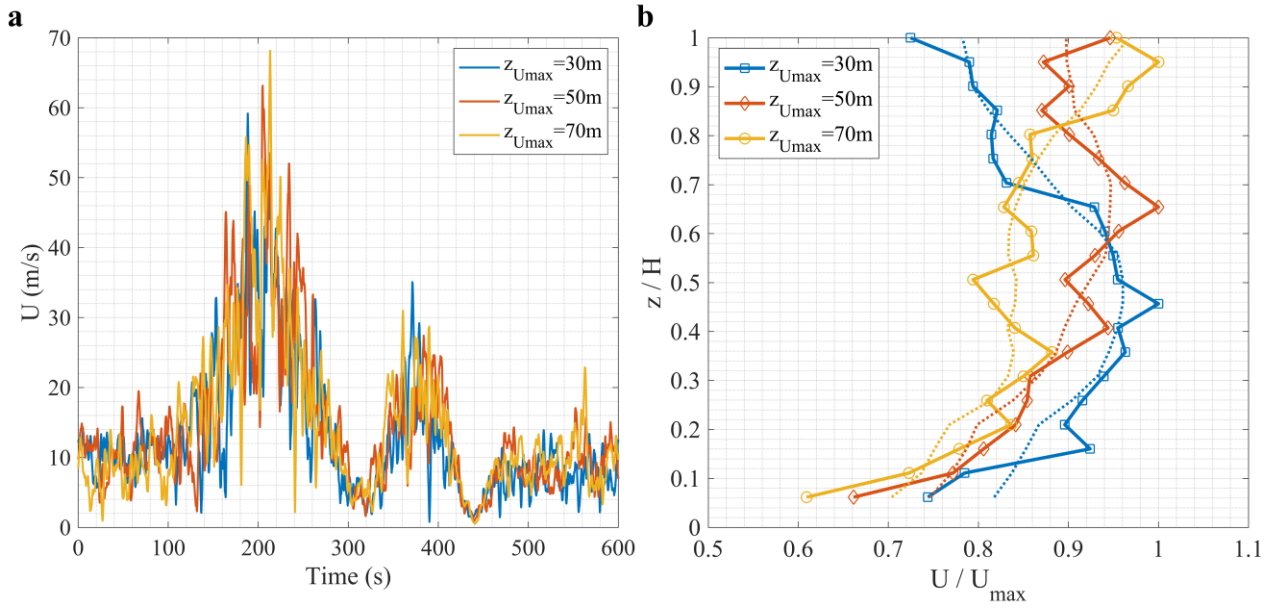

Figure 2. *Horizontal and vertical profiles of outflow velocity, (a) Horizontal velocity time history at the height of maximum velocity; (b) Peak velocity at each storey.*

3.4 Results and discussions

3.4.1 Transient non-stationary wind

Initially, the transient wind loads (i.e. profile 1-$z_{U_{max}}$= 30 m, profile 2-$z_{U_{max}}$= 50 m and profile 3-$z_{U_{max}}$= 70 m) are applied on the building model alone and the results are shown in Figure 3 (a1) - (a3). The deformations of the building are within the elastic range under downburst profile 1 and profile 3 since the ductility factor is less than 1, i.e. 0.91 and 0.95 (see Table 1). The corresponding distribution of stresses when the maximum displacement ductility occurs are shown in Figure 4 (a1) and Figure 4 (a3), which indicate that high stresses are concentrated on the 1st to 10th storeys of the building. A higher ductility demand can be observed under downburst profile 2, as shown in Figure 3 (a2). The structural deformation has entered to the plastic range and the maximum ductility demand is 1.57. The corresponding distribution of stresses when the maximum displacement ductility occurs is shown in Figure 4 (a2). Higher stresses are observed than those under profiles 1 and 3, which are concentrated on the 4th to 8th storeys and base of ground columns.

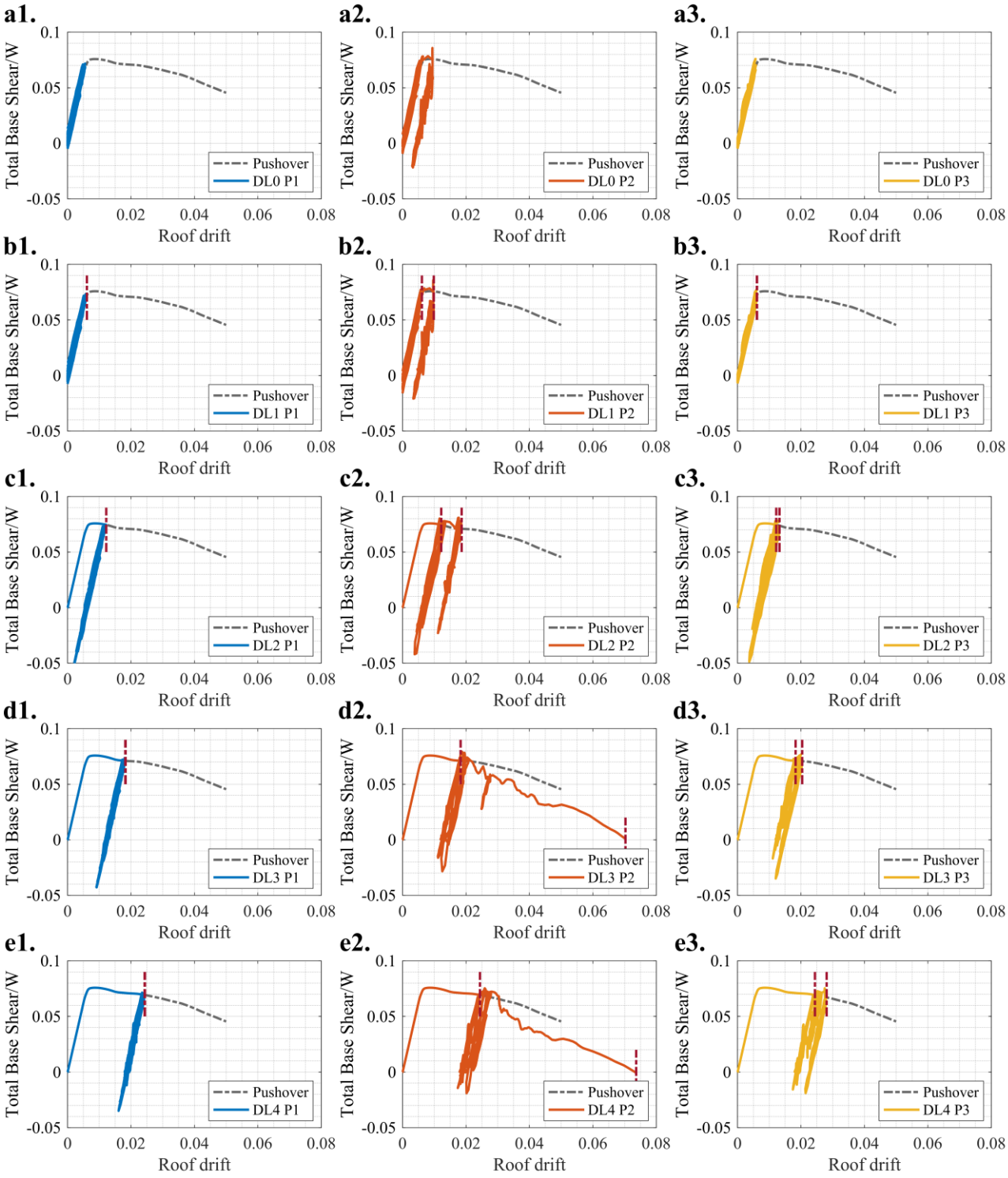

Figure 3. *Pushover curves under three profiles of downburst outflows, (a) Downburst; (b) DL1-Downburst; (c) DL2-Downburst; (d) DL3-Downburst; (e) DL4-Downburst (Red dash line represents the maximum displacement after the primary and secondary hazards separately).*

a1. DL0 Profile 1

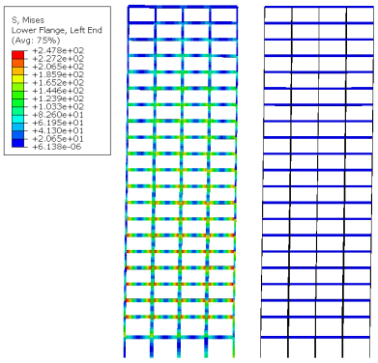

a2. DL0 Profile 2

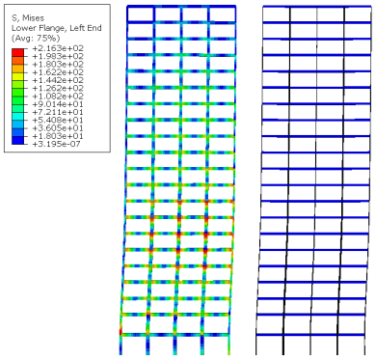

a3. DL0 Profile 3

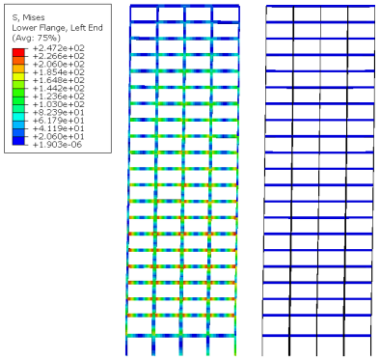

b1. DL1 Profile 1

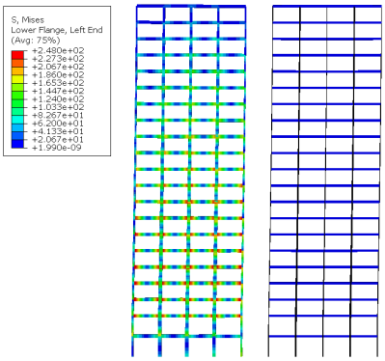

b2. DL1 Profile 2

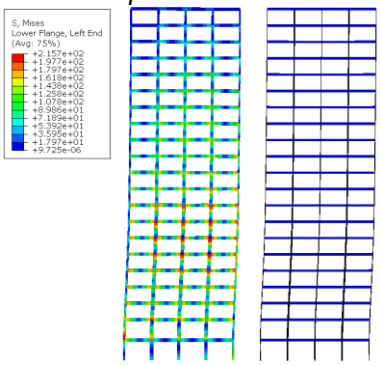

b3. DL1 Profile 3

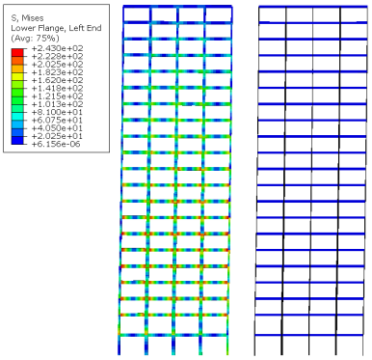

c1. DL2 Profile 1

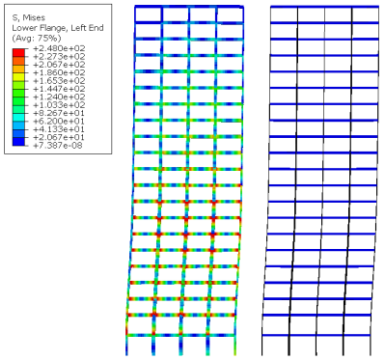

c2. DL2 Profile 2

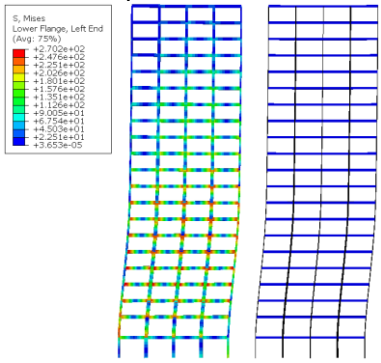

c3. DL2 Profile 3

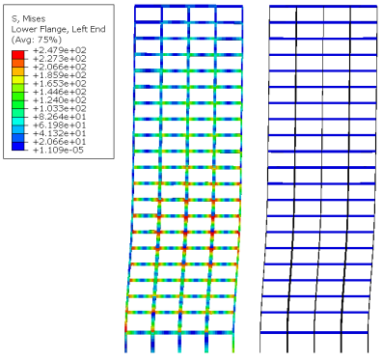

d1. DL3 Profile 1

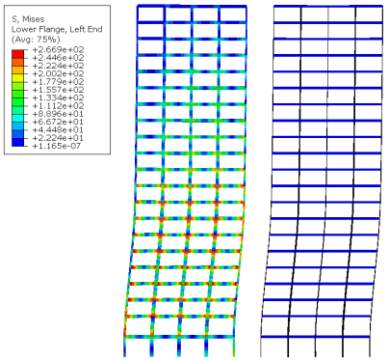

d2. DL3 Profile 2

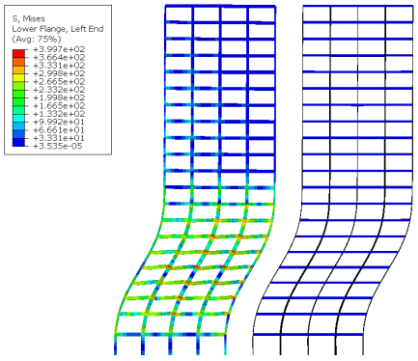

d3. DL3 Profile 3

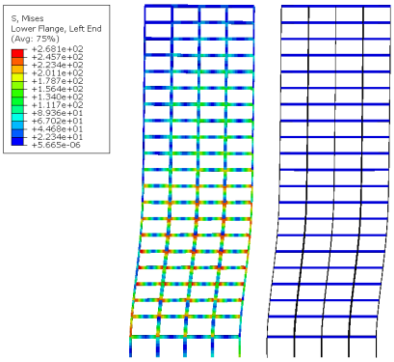

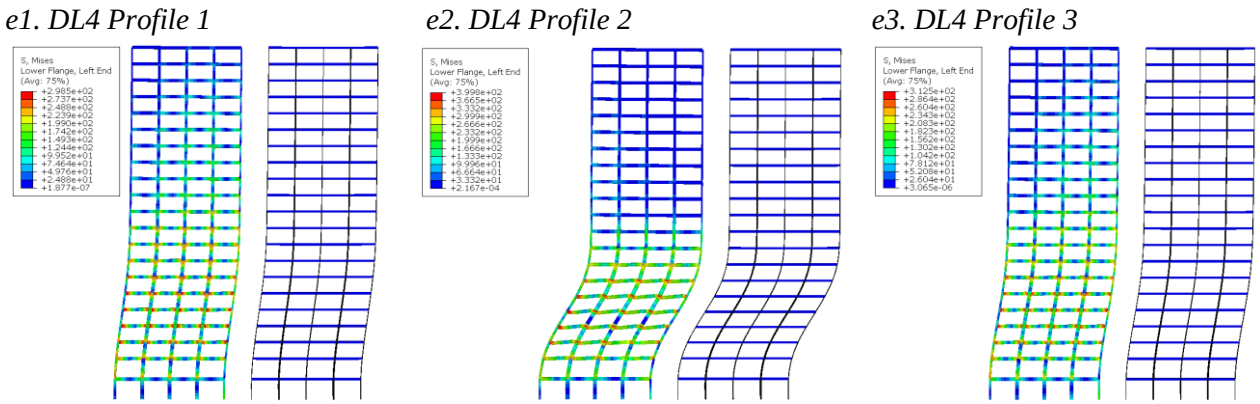

Figure 4. *Global Stress distribution at maximum displacement, (a) Downburst; (b) DL1-Downburst; (c) DL2-Downburst; (d) DL3-Downburst; (e) DL4-Downburst*

Table 1. *Ductility demand for different profiles.*

$Z_{U_{max}}$ *(m)*	30	50	70
DL0	0.91	1.57	0.95
DL1	1.00	1.62	1.01
DL2	2.00	3.05	2.17
DL3	2.98	11.52	3.34
DL4	3.98	12.07	4.60

3.4.2 Sequential multi-hazard analysis

The base shear - roof drift relationship for the sequential-hazard analysis is illustrated in Figure 3 (b) - (e). The three simulated downburst scenarios are applied to the damaged building which has already reached a target ductility level (i.e. DL1, DL2, DL3 and DL4). The maximum ductility demands of the sequential analysis are summarised in Table 1. In general, it can be seen from this table that as the initial target ductility level increases, the ductility demands of the sequential wind event tend to increase (see red dash line in Figure 3).

Under the sequential analysis of downburst profile 1, the structure responded within the elastic range (Figure 3 (b1) - (e1)). There might be some accumulation of fatigue damage, but this has not resulted in an increase of the roof displacement. The high-stress area is observed between 1st and 10th storey for the DL1 initial damage state and turns to be concentrated between 5th and 8th storey for the DL 2-4 initial damage states (see Figure 4 (b1) -(e1)). Under the sequential analysis of downburst profile 2, the structure responded inelastically and higher plastic deformations were observed than those during the initial pushover analysis. The maximum ductility was found to be 1.62 and 3.05 when the downburst event follows the DL1 and DL2 initial damage state, respectively. The high-stress area is located between the 4th and 8th storey of the building (See Figure 4 (b2) and (c2)). The ductility demands increase significantly when the downburst event follows the DL3 and DL4 initial damage state resulting in four- and three-times higher ductility demands than that of the primary event, i.e. 11.52 and 12.07, respectively (Figure 3 (d2) and Figure 3 (e2)). Excessive yielding areas have been formed and steel beams have reached their maximum tensile strength. Under these ductility levels, a collapse mechanism has been formed that involves the 2nd and 5th storey of the building, as shown in Figure 3 (d2) and Figure 3 (e2).

Under the sequential analysis of downburst profile 3, the structure responded inelastically but reached lower ductility levels than in the sequential analysis of downburst profile 2. The ductility demands increase to 1.01, 2.17, 3.34 and 4.60 when the downburst event follows the DL1, DL2, DL3 and DL4 ductility level of the primary event. The high-stress locations for profile 3 are similar as the profile 1.

The results of these three analysis profiles demonstrate that although the maximum velocity of the downburst occurs in profile 3 (70 m/s), the downburst wind profile 2 imposed higher ductility demands leading the structure to global collapse. These results indicate that the height at which the maximum wind velocity occurs

alongside with the shape of the vertical wind profile are two important parameters for consideration as they control the input energy and excessive plastic deformations of the structure. The proposed analysis method can successfully identify the capacity margins and collapse mechanism of structures under sequential hazard events and can be implemented to quantify the increased ductility demands within a multi-hazard assessment framework.

4. CONCLUSIONS

In this paper, a new algorithm has been proposed for the nonlinear analysis of the buildings under sequential hazard loads. The merit of this procedure is that the primary hazard analysis can stop at any pre-defined ductility level (i.e. single-hazard design) and the secondary hazard event can be applied as sequential event. This allows for a direct quantification of the additional ductility demands due to the secondary hazard event. This method is validated on a 20-storey steel building which consists of one exterior moment resisting frame and one interior equivalent gravity frame designed based on the 1994 Uniform Building Code. Three downburst synthetic records were applied as secondary hazard events having different vertical wind profiles and maximum wind velocity. The main conclusions of this study are as follows:

- The input energy from the sequential downburst event may drive the structure to plasticity thus exceeding the single-hazard ductility demands. The level of damage exhibited by the structure during the secondary hazard event increases with the ductility demands of the primary event.
- The multi-hazard analysis results demonstrated the importance of the height at which the maximum wind velocity occurs and that of the shape of the vertical wind profile. Both parameters control the input wind energy and determine the storeys in a structure that are prone to excessive plastic deformations.
- Under the sequential analysis of downburst profile 2, ductility demands increased significantly when the downburst event followed the DL3 and DL4 initial damage state resulting in four- and three-times higher ductility demands than that of the primary event, i.e. 11.52 and 12.07, respectively. Under these ductility levels, a collapse mechanism was formed that involved the 2nd and 5th storey of the building.
- The proposed analysis method can successfully identify the capacity margins and collapse mechanism of the structures under multi-hazards and can effectively quantify the increased ductility demands due to the sequential hazard event.

The limitation of this study is that the pressure coefficient used for calculating the wind load is independent of the height above the ground due to the insufficient recorded data for this parameter caused by downburst outflows on buildings. Real recorded thunderstorm downburst events are needed for further investigation.

REFERENCES

ABAQUS. (2020). User Documentation. In.

ABCNEWS. (2017). Hurricane Katia mudslide leaves two dead in Mexico after earthquake clean-up begins. Available at www.abc.net.au/news/2017-09-10/deadly-quake-hurricane-katia-a-one-two-punch-for-mexico/8889064 [Accessed on 20.09.17].

Aly, A. M.and Abburu, S. (2015). On the design of high-rise buildings for multihazard: fundamental differences between wind and earthquake demand. *Shock and Vibration, 2015*. doi:https://doi.org/10.1155/2015/148681

ASCE7. (2013). *Minimum Design Loads for Buildings and Other Structures (ASCE/SEI 7-10)*.

Brooks, H. E. (2013). Severe thunderstorms and climate change. *Atmospheric Research, 123*, 129-138. doi:https://doi.org/10.1016/j.atmosres.2012.04.002

Chen, L.and Letchford, C. (2004). A deterministic–stochastic hybrid model of downbursts and its impact on a cantilevered structure. *Engineering Structures, 26*(5), 619-629. doi:http://dx.doi.org/10.1016/j.engstruct.2003.12.009

Chopra, A. K.and Goel, R. K. (2002). A modal pushover analysis procedure for estimating seismic demands for buildings. *Earthquake engineering & structural dynamics, 31*(3), 561-582. doi:https://doi.org/10.1002/eqe.144

CNN. (2017). Mexico had two major earthquakes this month. Here's why. Available at http://edition.cnn.com/2017/09/20/americas/mexico-two-earthquakes-in-one-month/index.html [Accessed on 20.09.17].

Code, U. B. (1994). International conference of building officials (ICBO). *Whittier, CA*.

Deodatis, G. (1996). Simulation of ergodic multivariate stochastic processes. *Journal of Engineering Mechanics, 122*(8), 778-787. doi:http://dx.doi.org/10.1061/(ASCE)0733-9399(1996)122:8(778)
Duthinh, D.and Simiu, E. (2010). Safety of structures in strong winds and earthquakes: multihazard considerations. *Journal of Structural Engineering, 136*(3), 330-333. doi:https://doi.org/10.1061/(ASCE)ST.1943-541X.0000108
Elias, S., Rupakhety, R.and Olafsson, S. (2019). Analysis of a benchmark building installed with tuned mass dampers under wind and earthquake loads. *Shock and Vibration, 2019*. doi:https://doi.org/10.1155/2019/7091819
Fujita, T. T. (1985). *The downburst: Microburst and Macroburst*: The University of Chicago.
Fujita, T. T. (1990). Downbursts: meteorological features and wind field characteristics. *Journal of wind engineering and industrial aerodynamics, 36*, 75-86. doi:http://dx.doi.org/10.1016/0167-6105(90)90294-M
Hall, J. F. (2018). On the descending branch of the pushover curve for multistory buildings. *Earthquake engineering & structural dynamics, 47*(3), 772-783. doi:https://doi.org/10.1002/eqe.2990
Holmes, J. D.and Oliver, S. (2000). An empirical model of a downburst. *Engineering Structures, 22*(9), 1167-1172. doi:http://dx.doi.org/10.1016/S0141-0296(99)00058-9
Isobe, D.and Tanaka, S. (2021). Sequential Simulations of Steel Frame Buildings Under Multi-Phase Hazardous Loads During a Tsunami. *Frontiers in built environment, 7*, 69.
Kwag, S., Gupta, A., Baugh, J.and Kim, H.-S. (2021). Significance of multi-hazard risk in design of buildings under earthquake and wind loads. *Engineering Structures, 243*, 112623. doi:https://doi.org/10.1016/j.engstruct.2021.112623
Li, Q.and Ellingwood, B. R. (2007). Performance evaluation and damage assessment of steel frame buildings under main shock–aftershock earthquake sequences. *Earthquake engineering & structural dynamics, 36*(3), 405-427.
Lombardo, F. T., Smith, D. A., Schroeder, J. L.and Mehta, K. C. (2014). Thunderstorm characteristics of importance to wind engineering. *Journal of wind engineering and industrial aerodynamics, 125*, 121-132. doi:http://dx.doi.org/10.1016/j.jweia.2013.12.004
Loredo-Souza, A. M., Lima, E. G., Vallis, M. B., Rocha, M. M., Wittwer, A. R.and Oliveira, M. G. (2019). Downburst related damages in Brazilian buildings: Are they avoidable? *Journal of wind engineering and industrial aerodynamics, 185*, 33-40. doi:https://doi.org/10.1016/j.jweia.2018.11.022
Martinez-Vazquez, P., Gkantou, M.and Baniotopoulos, C. (2019). Strength and ductility demands on wind turbine towers due to earthquake and wind load. *Proceedings of the Institution of Civil Engineers-Structures and Buildings, 172*(8), 556-563. doi:https://doi.org/10.1680/jstbu.17.00154
MATLAB. (2021). https://www.mathworks.com/help/pdf_doc/matlab/rn.pdf.
Melbourne, W. (1980). Comparison of measurements on the CAARC standard tall building model in simulated model wind flows. *Journal of wind engineering and industrial aerodynamics, 6*(1-2), 73-88. doi:https://doi.org/10.1016/0167-6105(80)90023-9
Park, S., van de Lindt, J. W., Cox, D., Gupta, R.and Aguiniga, F. (2012). Successive earthquake-tsunami analysis to develop collapse fragilities. *Journal of Earthquake Engineering, 16*(6), 851-863.
Priestley, M. B. (1965). Evolutionary spectra and non‐stationary processes. *Journal of the Royal Statistical Society: Series B (Methodological), 27*(2), 204-229. doi:https://doi.org/10.1155/2015/945203.
Rädler, A. T., Groenemeijer, P. H., Faust, E., Sausen, R.and Púčik, T. (2019). Frequency of severe thunderstorms across Europe expected to increase in the 21st century due to rising instability. *npj Climate and Atmospheric Science, 2*(1), 1-5. doi:https://doi.org/10.1038/s41612-019-0083-7
Skalomenos, K. A.and Papazafeiropoulos, G. (2019). A computational method for performing nonlinear adaptive pushover analysis of structures through ABAQUS simulation. *Proceedings of 7th COMPDYN. Heraklion, Crete, Greece*. doi: https://doi.org/10.7712/120119.7199.19194
Solari, G., Burlando, M., De Gaetano, P.and Repetto, M. P. (2015). Characteristics of thunderstorms relevant to the wind loading of structures. *Wind and Structures, 20*(6), 763. doi:http://dx.doi.org/10.12989/was.2015.20.6.763
Solari, G., De Gaetano, P.and Repetto, M. P. (2013). *Wind loading and response of structures in mixed climates.* Paper presented at the Proceedings of the Eight Asia Pacific Conference on Wind Engineering.
Taha, A. (2021). Vibration Control of a Tall Benchmark Building under Wind and Earthquake Excitation. *Practice Periodical on Structural Design and Construction, 26*(2), 04021005. doi:https://doi.org/10.1061/(ASCE)SC.1943-5576.0000569
Thilakarathna, S. N., Anwar, N., Norachan, P.and Naja, F. A. (2018). The effect of wind loads on the seismic performance of tall buildings. *Athens Journal of Technology & Engineering, 5*(3), 251-276. doi:https://doi.org/10.30958/ajte.5-3-3
Tilloy, A., Malamud, B. D., Winter, H.and Joly-Laugel, A. (2019). A review of quantification methodologies for multi-hazard interrelationships. *Earth-Science Reviews, 196*, 102881. doi:https://doi.org/10.1016/j.earscirev.2019.102881
Wood, G. S., Kwok, K. C., Motteram, N. A.and Fletcher, D. F. (2001). Physical and numerical modelling of thunderstorm downbursts. *Journal of wind engineering and industrial aerodynamics, 89*(6), 535-552. doi:http://dx.doi.org/10.1016/S0167-6105(00)00090-8